Comprehensive Annotation of the *Parastagonospora nodorum* Reference Genome Using Next-Generation Genomics, Transcriptomics and Proteogenomics

Robert A. Syme[1©], Kar-Chun Tan[1©], James K. Hane[1,2©], Kejal Dodhia[1], Thomas Stoll[3], Marcus Hastie[3], Eiko Furuki[1], Simon R. Ellwood[1], Angela H. Williams[1], Yew-Foon Tan[4], Alison C. Testa[1], Jeffrey J. Gorman[3], Richard P. Oliver[1] *

1 Centre for Crop & Disease Management, Department of Environment and Agriculture, Curtin University, Bentley, WA, Australia, 2 Curtin Institute for Computation, Curtin University, Bentley, WA, Australia, 3 Protein Discovery Centre, QIMR Berghofer Medical Research Institute, Herston, Qld, Australia, 4 Telethon Kids Institute, Subiaco, WA, Australia

© These authors contributed equally to this work.
* Richard.Oliver@curtin.edu.au

Abstract

Parastagonospora nodorum, the causal agent of Septoria nodorum blotch (SNB), is an economically important pathogen of wheat (*Triticum* spp.), and a model for the study of necrotrophic pathology and genome evolution. The reference *P. nodorum* strain SN15 was the first Dothideomycete with a published genome sequence, and has been used as the basis for comparison within and between species. Here we present an updated reference genome assembly with corrections of SNP and indel errors in the underlying genome assembly from deep resequencing data as well as extensive manual annotation of gene models using transcriptomic and proteomic sources of evidence (https://github.com/robsyme/Parastagonospora_nodorum_SN15). The updated assembly and annotation includes 8,366 genes with modified protein sequence and 866 new genes. This study shows the benefits of using a wide variety of experimental methods allied to expert curation to generate a reliable set of gene models.

Background

Although the cost of DNA sequencing has decreased to the point where it no longer represents a significant hindrance to obtaining an initial assembly, [1] an accurately annotated eukaryotic genome remains a significant challenge. Genome assembly can be hampered by errors arising from sequencing errors or the presence of repetitive regions, which can lead to truncated contigs and a fragmented assembly. Genes and other features are typically annotated using homology-based methods or are predicted *ab initio*. Experimental gene validation techniques are required to complement *in silico* methods to obtain high quality gene model annotations.

Parastagonospora nodorum [teleomorph: *Phaeosphaeria* (Hedjar.) syn. *Leptosphaeria nodorum* (Müll.), syn. *Septoria nodorum* (Berk.), syn. *Stagonospora nodorum* (Berk.)] is a filamentous Ascomycete and member of the Dothideomycetes, a taxonomic class that includes several agriculturally-damaging phytopathogens [2–5]. *P. nodorum* causes the wheat disease Septoria nodorum blotch (SNB, syn. glume blotch) [6] and is responsible for substantial yield losses in many regions around the world. As part of the infection process, the fungus produces an arsenal of proteinaceous effectors that induce tissue necrosis and/or chlorosis on hosts expressing the corresponding susceptibility gene [7]. Analysis of the *P. nodorum* / wheat pathosystem has revealed the role of necrotrophic effectors SnToxA [8], SnTox1 [9] and SnTox3 [10] in conferring virulence. The presence of undiscovered effectors in *P. nodorum* is evident by observation of SNB QTLs in wheat cultivars when challenged with culture filtrate [11] from the reference strain devoid of known effector genes [12] or from other *P. nodorum* strains [3]. In addition to effectors, *P. nodorum* genes involved in primary metabolism, secondary metabolism, and signal transduction have been studied to elucidate their involvement in the *P. nodorum* pathogenic lifecycle. Characterised metabolic enzymes include malate synthase [13], δ-aminolevulinic acid synthase [14], pantoate-β-alanine ligase [15], trehalose 6-phosphate synthase [16] and components of mannitol metabolism [6, 17]. *P. nodorum* signal transduction and regulatory genes that have been studied in depth include the transcription factor *StuA* [18], a MAP kinase [19], calcium/calmodulin-dependent protein kinases [20], a putative short-chain dehydrogenases [21, 22] revealed to be necessary for the formation of the mycotoxin alternariol and sporulation [23] and those with a role in cyclic AMP signalling [24, 25].

The first published Dothideomycete whole genome assembly was of *P. nodorum* strain SN15. The original sequence was obtained in 2004 using 1 Kb, 4 Kb, and 40 Kb Sanger shotgun-sequenced paired reads assembled as 37.1 Mb of nuclear DNA in 107 scaffolds and the complete 49.8 Kb mitochondrial genome [26]. Initial gene-structure annotation relied heavily on automated methods, but was subsequently revised after analysis of proteogenomic [27], and microarray data [28] to give a total of 10,761 gene models with a mean exon count of 2.6, mean CDS length of 1,400 bp, mean intergenic distance of 1,685 bp, and a mean intron length of 91 bp. Repetitive sequence comprised 4.52% of the genome in 5 subtelomeric repeat classes, 1 ribosomal DNA repeat and 20 transposon or transposon-like clusters [29]. Repeat-induced point (RIP) mutations in repeat instances were subsequently *in-silico* reversed to allow classification of the repeat X26 as a RecQ helicase, R25 as a pseudogene, and repeats X3 and X8 as members of the same ancestral class [30].

The genomics resources available to *P. nodorum* researchers were expanded to include the genomes of two more strains—one isolated from the grass *Agropyron* that is unable to infect wheat, and a wheat-pathogenic isolate known to produce a different suite of effectors to the SN15 reference strain. In comparing the three strains, Syme et al. [31] added 1,621 'lower-confidence genes' to the 10,761 genes from Bringans et al. [27] to minimise the possibility of missing potential effector loci, bringing the total number of putative genes used in that comparison to 12,382. Clustering of the predicted proteomes from the three strains revealed a core set of 10,464 conserved proteins and 2,421 putative proteins that were exclusive to strains able to infect wheat [31].

The initial SN15 assembly was found to contain a homolog of the *Pyrenophora tritici-repentis* necrotrophic effector ToxA, providing evidence of a horizontal gene transfer event from *P. nodorum* to *P. tritici-repentis* [8]. The *ToxA*-containing transfercon was initially estimated to be 11 Kb, however we propose that a larger region of at least 72 to 145 Kb was transferred [31, 32], corresponding to *P. nodorum* scaffolds 68, 55, 51, 46, 64, and 73.

The accuracy and completeness of a genome assembly can be improved by the addition of new sequencing data as error characteristics and shortcomings of one sequencing technique

may be overcome by a complementary chemistry [33, 34]. The long read lengths available from Sanger sequencing have been useful to resolve repetitive regions and provide the large-scale structural assembly for SN15, however the depth and accuracy of additional Illumina short-reads could be used to correct remaining SNPs and small insertions or deletions [35]. Similarly, the quality of predicted gene models can be improved by the addition of transcriptomic and proteomic data sources by correction of errors in intron/exon boundaries and the revelation of new loci not previously known to be transcribed [27, 36].

Comparison of the chromosomes of filamentous ascomycetes have shown that related chromosomes tend to conserve gene content, but with shuffled gene order [37]. The resulting syntenic patterns are described as 'mesosynteny' and can be explained by frequent chromosomal inversions but infrequent translocations [37, 38]. Mesosyntenic patterns may also be utilized to resolve the order and orientation of scaffolds in a fragmented genome assembly and thereby identify groups of scaffolds that comprise a single chromosome [37]. The utility of this technique is most obvious when a reliable 'finished' genome can be used to improve a fragmented 'draft' assembly of a closely related species or strain.

This study offers greatly improved genome assembly and gene model annotation datasets for *P. nodorum* SN15 than the previous update described in Bringans et al. [27]. We report extensive correction of SNP and indel base-calling errors in the *P. nodorum* SN15 reference assembly, the closing of assembly gaps, extensive automated and manual gene annotation, and improvements to the functional characterisation of gene models. The new experimental data comprises RNA sequencing, DNA sequencing, and multiple sets of proteomic data which were used to inform comprehensive manual curation of gene models. Using these complementary approaches, we have generated a greatly improved genome assembly, and have re-predicted the gene and protein datasets including potential pathogenicity effector genes. These bioinformatic resources represent a substantial knowledge-base that will support future research in Dothideomycete genome biology.

Methods

Fungal culture

P. nodorum SN15 was maintained on V8-PDA medium. For the induction of extracellular proteins, 1×10^6 *P. nodorum* SN15 spores were grown in Fries broth [39]. For genomic DNA, RNA and protein extraction experiments involving the intracellular and cell-wall/membrane sub-proteomes, 1×10^6 *S. nodorum* SN15 spores were grown in minimal medium broth for 3 days [22]. The mycelium was harvested and freeze-dried prior to further manipulations.

Genomic DNA extraction and Illumina sequencing

P. nodorum SN15 genomic DNA was extracted using a modified high-salt cetyltrimethylammonium bromide (CTAB) protocol [40]. Briefly, freeze-dried mycelia were ground to a fine powder using a chilled mortar and pestle. Genomic DNA was extracted using an extraction buffer that consisted of 100 mM Tris, 50 mM EDTA, 2M NaCl, 0.4% (v/v) β-mercaptoethanol, 2% (w/v) polyvinylpyrrolidone and 2% (w/v) CTAB. The genomic DNA was subjected to phenol/chloroform extraction, ethanol precipitation and washes. A paired-end library with an average insert size of 439 bp and read lengths of 100 bp was generated from SN15 genomic DNA and used for sequencing. Sequencing of the genomic DNA was carried by the Australian Genome Research Facility (Melbourne, Australia) using an Illumina HiSeq 2000 (Illumina, CA, USA).

RNA extraction and Illumina sequencing

P. nodorum SN15 total RNA was extracted using the Trizol reagent (Invitrogen, CA, USA) and DNase-treated. PCR was used to check that the sample was free of genomic DNA [41]. RNA sequencing was carried out by Macrogen (Seoul, South Korea) using an Illumina HiSeq 2000.

Raw Illumina sequencing reads were inspected with FastQC [42]. Adapter sequence and low quality terminal sequences were removed with Cutadapt v1.0 [43]. Parameters and run details are available in S1 Text.

Proteomic datasets

The extracellular proteome was extracted as described by Vincent et al. [44], using a modified tricholoacetic acid (TCA)/acetone protein precipitation procedure. Briefly, proteins from the extracellular culture filtrate were precipitated, collected by centrifugation and washed with 100% acetone. The protein pellet was subsequently air-dried at room temperature and suspended in 20 mM Tris pH 7. Residual TCA was progressively removed by dialysis of the suspension using D-Tube Dialyzer Maxi, MWCO 3.5 kDa (Novagen, Darmstadt, Germany) in several changes of 20 mM Tris pH 7 at 4°C for 48 hrs. Solubilised proteins were retained and stored at -80°C until further manipulation.

The intracellular proteome was extracted as previously described by the authors of this study [41]. Briefly, intracellular proteins from mechanically ground freeze-dried mycelia were solubilised in 20 mM Tris-Cl pH 7 and de-salted using a PD10 chromatography column (GE Healthcare, Little Chalfont, UK). Solubilised proteins were retained and stored at -80°C until required.

To facilitate cell wall/membrane (CWM) proteome extraction, freeze-dried fungal mycelia were ground with a mortar and pestle and washed three times with 20 mM Tris-Cl pH 7 to release and remove soluble intracellular proteins. The pellet was then washed three times with 0.1 M Na_2CO_3 to further remove soluble and peripherally-attached proteins. The pellet was then resuspended in 20 mM Tris-Cl pH 7 and subjected to 3 cycles of slow freeze and thaw to further break up the cellular material. Membrane-bound proteins were extracted using two methods: Extraction Procedure 1 (EP1)– 100 mg of membrane enriched pellet was extracted with 2% (w/v) SDS, 100 mM EDTA and 50 mM DTT in 100 mM Tris/HCl (pH7.8) by vortexing and boiling for 5 min followed by 5 min on ice (based on methods presented in Meijer et al., 2006 and Feiz et al., 2006); Extraction Procedure 2 (EP2)– 100 mg of membrane enriched pellet was extracted with 2% (w/v) SDS, 7 M urea, 2 M thiourea and 50 mM DTT in 125 mM triethylammonium bicarbonate (TEAB, pH 8.5) by vortexing and sonication for 15 min in an ice-cold sonication bath followed by resting for 30 min on ice. Vortexing and sonication steps were repeated. Subsequent sample processing for suspensions derived from 'Extraction Procedures' EP1 and EP2 were identical. Suspensions were centrifuged at 16,000 x g for 5 min (4°C) and the supernatants removed. Pellets were washed twice with either 100 mM Tris/HCl (pH 7.8) for EP1 or 100 mM TEAB (pH 8.5) for EP2. Respective supernatants were pooled, centrifuged at 20,000 x g for 15 min (4°C) and collected for further processing. Proteins were precipitated from supernatants by the addition 100% TCA to a final concentration of 20% (v/v) and incubated on ice for 30 min. Protein precipitates were harvested by centrifugation at 20,000 x g for 10 min (4°C). Pellets were washed twice with 90% (v/v) acetone and centrifuged each time as before. Protein pellets were briefly dried under a gentle stream of nitrogen and used immediately. The final pellets were re-suspended in 45 µL of EP2 extraction buffer (without DTT) and 5 µL of 1 M TEAB (pH 8.5) by repeated vortexing and incubating the tubes for 10 min in an ice cold sonication bath. Samples were centrifuged at 20,000 x g for 10 min (4°C) and supernatants collected for further processing. Protein concentration of all samples was determined using the

2D-Quant kit (GE Healthcare) according to the manufacturer's 'Standard procedure' protocol. CWM proteins were digested without prior fractionation.

Intracellular and extracellular proteins were separated into 24 fractions using isoelectric point-based fractionation of proteins (Agilent 3100 Offgel fractionator) with liquid-phase recovery followed by digestion and LC-MS analysis of peptides. Offgel separations were performed using high resolution separation kits (pH range 3–10, 24 cm IPG gel strips; Agilent) and approx. 1 mg of protein per strip loading as described previously [45]. The pH of 100 μL aliquots of recovered Offgel fractions was adjusted by adding 10 μL of 1 M TEAB (pH 8.5). CWM sample aliquots of 80 μg protein were diluted with 10 μL of 1 M TEAB (pH 8.5) and the volume adjusted to 110 μL with EP2 extraction buffer (without DTT).

Proteins were reduced with 5 μL of 0.5 M tris(2-carboxyethyl)phosphine (TCEP, 22 mM final conc.) for 2.5 hours at 4°C and then alkylated with 16 μL of 1 M iodoacetamide (122 mM final conc.) in the dark at 22°C for 2 hours. Reducing agent TCEP was dissolved in 100 mM TEAB (pH 8.5) and neutralised with 10 M sodium hydroxide solution to pH 8. Sample proteins were co-precipitated with 1 μg of modified trypsin (Roche, sequencing grade) by adding 10 volumes of methanol as follows: One microliter of trypsin was added to the side of the Eppendorf tube and quickly flushed into the sample solution with 1.3 mL of 100% methanol at -20°C. Tubes were incubated overnight at -20°C. Protein precipitates were harvested by centrifugation at 20,000 x g for 15 minutes (4°C). Pellets were washed twice, once with 1 mL of 90% (v/v) methanol at -20°C and finally with 1 mL of 100% methanol at -20°C and centrifuged each time as before. Protein pellets were briefly dried under a gentle stream of nitrogen and continued immediately. The final pellets were re-suspended in 40 μL of 100 mM TEAB buffer (pH 8.5) containing 5% acetonitrile by repeated vortexing and incubating the tubes for 1 min in the sonication bath. Samples were incubated at 37°C for 2 hours followed by the addition of further 1 μg of modified trypsin and 6 hours (Offgel fractions) and 14 hours (CWM proteome) digestion at 37°C. Protein digests were stored at -80°C until analysis.

For LC-MS/MS analysis, trypsin-digested samples were centrifuged for 5 min at 20,000 x *g* and an aliquot of 5 μL (Offgel fractions) or 3 μL (CWM proteome) was diluted to a volume of 20 μL with 6.5% formic acid prior to injection. Tryptic peptides were separated on a Prominence nano HPLC system (Shimadzu, Kyoto, Japan) and data collected on a Hybrid LTQ Orbitrap mass spectrometer (Thermo Fisher Scientific, Bremen, Germany). Mobile phases for chromatographic peptide separation were as follows: Eluent A was milliQ water containing 0.1% formic acid and eluent B was 80% acetonitrile / 20% milliQ water (v/v) containing 0.1% formic acid.

Acidified Offgel fractions were loaded onto a reversed-phase trap column (Dionex Acclaim PepMap μ-Precolumn C18, 0.3 mm x 5 mm) at 30 μL/min in 100% eluent A for 3.5 minutes and subsequently separated on a reversed phase capillary column (Vydac Everest C18 5μm 300 Å, 150 μm x150 mm, Alltech) at 45°C and a flow rate of 1 μL/min. Separation was performed with gradients of 2–30% B over 60 and 90 minutes (depending on sample complexity), followed by a 95% B wash step, resulting in a total run time of 110 and 140 minutes, respectively. Data was either acquired on an LTQ Orbitrap Velos as outlined below or an LTQ Orbitrap XL as described in Hastie et al. [45] with the following modifications to data acquisition: target value of 1 x 10^3 for ion trap MS/MS scans; dynamic exclusion set to 70 s; ion selection threshold 1000 counts.

Acidified CWM digests were loaded onto a reversed-phase trap column (ReproSil-Pur C18-AQ 3μm, 0.3 mm x 10 mm; Dr. Maisch, Ammerbuch-Entringen, Germany) and washed for 3.5 minutes at 30 μL/min using 100% eluent A. Peptide mixtures were subsequently back flushed onto a capillary column (150 μm x 150 mm) packed in-house with reversed-phase beads (ReproSil 100 C18 3μm; Dr. Maisch) and separated at a flow rate of 1 μL/min. Peptides

were separated at 55°C using a sequence of linear gradients: to 5% B over 3.5 minutes; to 35% B over 166.5 minutes; to 45% B over 10 minutes; to 95% B over 10 minutes and then holding the column at 95% B for 10 minutes. Data was acquired on an LTQ Orbitrap Velos Pro as described below.

Column-separated peptides were electrosprayed into the LTQ Orbitrap Velos and LTQ Orbitrap Velos Pro through a Nanospray Flex Ion Source (Thermo Fisher Scientific) using 30 μm inner diameter uncoated silica emitter (New Objective). Spray voltage was 1.5 kV with no sheath, sweep or auxiliary gases used. The heated capillary temperature was set to 250°C and 285°C for the LTQ Orbitrap Velos and LTQ Orbitrap Velos Pro, respectively. An S-lens value of 50 to 55% was used.

The LTQ Orbitrap Velos (OT Velos) and LTQ Orbitrap Velos Pro (OT Velos Pro) were controlled using Xcalibur 2.2 software (Thermo Fisher Scientific) and operated in data-dependent acquisition mode to automatically switch between Orbitrap-full scan MS and ion trap-MS/MS acquisition. Full scan MS spectra (OT Velos: *m/z* 300–2000; OT Velos Pro: *m/z* 380–1700) were acquired in the Orbitrap mass analyser with a resolving power set to 30,000 (OT Velos) and 60,000 (OT Velos Pro) at 400 *m/z* after accumulation to a target value of 1×10^6 in the linear ion trap. The top 20 (OT Velos) and 15 (OT Velos Pro) most intense ions with charge states $\geq$ +2 were sequentially isolated with a target value of 5,000 and fragmented using collision-induced dissociation (CID) in the linear ion trap. 'Rapid' scan mode was selected for the ion trap- MS/MS acquisition in the OT Velos Pro. Fragmentation conditions were set as follows: 35% normalized collision energy; activation q of 0.25; 10 ms activation time; ion selection threshold 1000 (OT Velos) and 5000 (OT Velos Pro) counts. Maximum ion injection times were 200 ms for survey full scans and 50 ms for MS/MS scans. Dynamic exclusion was set to 70 s and 90 s for OT Velos and OT Velos Pro runs, respectively. Lock mass of *m/z* 445.12 was applied with an abundance was set at 0%.

Mass spectra were then searched using the Tide search engine [46] implemented in the Crux toolkit [47] with specifications as follows: spectra mapped against: 6-frame translations of both the new and the old genome assemblies and the set of predicted protein sequences from both the new and the old annotations. The search parameters used were: variable modifications, oxidation (M); and deamidation (NQ); fixed modification, carbamidomethyl (C); peptide tolerance, 20 ppm; MS/MS tolerance: ±0.8 Da; Digestion enzyme: trypsin; maximum missed cleavages: 1. Peptide-spectrum matches were refined using Percolator [48], again as implemented in the Crux toolkit.

For 1D-LC MALDI MS/MS analysis of the SN15 extracellular proteome, SN15 trypsin-digested peptides were resuspended in 20 μl of 2% acetonitrile and 0.05% trifluoroacetic acid. Peptides were loaded onto a C18 PepMap100, 3 mm column (Dionex, CA, USA) through the Ultimate 3000 nano HPLC system (Dionex, CA, USA). Mass spectrometry analysis was carried out on a 4800 MALDI TOF/TOF Analyser as previously described [49]. These spectra were also searched using the Tide search engine [46] with specifications: variable modifications, oxidation (M); fixed modification, carbamidomethyl (C) and other parameters and post-processing as above.

Conflicts with existing annotations were identified where proteomic spectra searched against the six-frame translation of the genome mapped into intergenic regions, intronic annotations or coding regions in the wrong frame.

Improvements to the SN15 Genome Assembly

SNP and indel errors in the *P. nodorum* SN15 assembly sequence [29] were corrected by MIRA (v3.4.1.1) [35], using its mapping algorithm to assemble Illumina gDNA reads onto the pre-

existing scaffolds. The original Sanger-sequenced reads were also re-mapped to the corrected assembly using BWA v0.7.3a-r367 [27]. Groups of putative scaffold linkage groups were predicted by comparison to *Pyrenophora tritici-repentis* [32] using the synteny-based cumulative binomial test for mesosynteny described by Hane et al. [37].

In order to assess the outcomes of genome sequence and gene annotation corrections, various diagnostic tests were performed. Changes made to the corrected genome were calculated with the dnadiff tool distributed with MUMmer [50]. Improvements of WGS read mapping to the corrected assembly were calculated by alignment with BWA v0.7.5a-r405 using the default parameters and summary statistics calculated with Picard v1.9.4 [51]. Improvements of RNA read mapping to the corrected assembly were calculated by alignment with TopHat v2.0.12 [52] and summary statistics calculated from TopHat reports and with Picard.

Improvements to the Genome Annotations

Errors in *P. nodorum* SN15 gene annotations were corrected using a combination of supporting data from RNA-seq and proteogenomic peptide alignments to the corrected assembly. RNA-seq reads were mapped to the corrected genome using TopHat v2.0.8 [52]. Manual correction of gene models and was performed using WebApollo [53]. JBrowse [54], through WebApollo was used to visualise the various '-omics' data sources that informed the manual correction.

RNA sequencing reads were aligned to the genome, and the gene models identified by Bringans et al. [27] were checked to ensure they matched all introns supported by 5 or more RNA-seq reads. Introns were introduced or removed from the annotations to match the RNA-seq data. New genes were annotated where transcription levels exceeded 5X when a suitable open reading frame (ORF) could be found and/or the ORF included at least one conserved domain as predicted by InterProScan using the–pathways and–goterms arguments and default parameters otherwise. Gene annotations were split when the RNA-seq depth dropped to 0 and/or the concatenated protein's BLAST hits showed two moieties of hit coverage. RNA-seq depth was also used to correct events where an ORF occurred inside the intron of another gene. These events were identified by large changes in read depth at a single locus. For each intronic insertion annotation, the translated region of the splice site skipping over the internal ORF was checked for consistency with blast results and with InterProScan-predicted domains spanning the splice site.

Exported and cleaned GFF3 and FASTA files were checked into git version control for distributed backup, sharing and review (https://github.com/robsyme/Parastagonospora_nodorum_SN15). Genome-wide support for gene annotations was summarised according to evidence type, requiring 80% coverage of coding sequence length and 5X coverage for RNA-seq support, peptides mapping within the coding region for proteogenomic support and four or more for microarray probes showing with expression levels at or above the cut-off determined by Ipcho et al. [15].

All gene annotations were manually reviewed and curated using the WebApollo platform, checking for consistency with RNA-seq, proteomics, microarray, BLAST hits against nr and conserved protein domain structures. Matches to conserved protein domains identified from translated gene models using InterProScan v5.8–49.0 [55] were compared between previously published and corrected datasets. Each protein set was submitted to dbCAN [56] for CAZyme enzyme family identification. GO functional annotations assigned by InterProScan were analysed for functional enrichment of the new protein set using the Fisher's test implemented in the goatools package [57].

Annotation and Comparison with Alternate Strains

P. nodorum strains SN4 and SN79 were re-annotated using Maker v2.31.8 [58]. Evidence supplied to Maker included the updated SN15 protein set and *ab-initio* predictions from the ab-initio mode of gene predictor CodingQuarry [59] using parameters generated from training on the updated SN15 annotations. The predicted protein set from the three *P. nodorum* strains were clustered using ProteinOrtho v5.11 [60] using the synteny option. Execution of parts of this analysis, including ProteinOrtho clustering, were aided by GNU parallel [61] and BioRuby scripts and gems [62, 63].

Results

Genome Assembly Sequence Correction

The genome of *P. nodorum* SN15 was re-sequenced using 100 bp paired-end Illumina libraries yielding 11.0 Gbp of raw sequence data equivalent to approximately 290x coverage. Short-reads were reassembled using the MIRA mapping algorithm to resolve or remove 37,501 Ns and correct 12,911 SNPs, 1,005 deletions, and 16,820 insertions (Table 1).

The genome annotations as described by Bringans et al. [27] were supplied as input to the MIRA assembly so that gene coordinates and identifiers could be preserved despite the correction of insertions and deletions to the underlying assembly.

The corrected genome sequence allowed for an additional 726 Kb of DNA reads to be mapped. Similarly, an additional 4,970 Mb of RNA reads were mapped to the corrected assembly. The reads mapped with lower rates of mismatch (0.4851% for DNA), and insertions/deletions (0.0062% for DNA and 0.0043% for RNA). The number of reads mapping in concordant pairs increased to 99.6% for DNA and 96.1% for RNA (Table 1).

Proteomic mass-spectral peptide matches from extracellular, cell-wall/membrane-bound and intracellular protein fractions were pooled and matches isolated by more than 200 bp from another match were discarded as likely false-positives. Existing annotations were checked for

Table 1. Summary of corrections made to the *P. nodorum* SN15 genome assembly.

Description	Before	After	Change
Number of nuclear scaffolds	107	91	-16
SNP changes	0	12,911	12,911
Single bp insertion corrected[a]	0	16,820	16,820
Single bp deletion corrected[b]	0	1,005	1,005
Unknown N sequences (bp)	164,388	126,887	-37501
WGS Reads mapping to genome ($\geq$Q20)	93,867,773	94,594,136	726,363
WGS read mismatch rate (%)[c]	0.5623	0.4851	-0.0772
WGS indel rate (%)[d]	0.0615	6.2e-03	-0.0553
WGS reads aligned in pairs (%)[e]	99.6402	99.6427	2.5e-3
RNA Reads mapping to genome ($\geq$Q20)	5,872,361,103	10,842,396,864	4,970,035,761
RNA indel rate (%)[d]	0.0348	0.0043	-0.0305
RNA reads aligned in pairs (%)[e]	95.0119	96.1274	1.1155

[a] deletion of erroneous sequence from the original assembly.

[b] insertion of sequence missing from the original assembly.

[c] rate of mismatched based relative to the reference sequence over all aligned regions.

[d] number of short insertions/deletions observed in reads / total aligned bases.

[e] percentage of reads with aligned mate pair.

doi:10.1371/journal.pone.0147221.t001

Table 2. New scaffold joins improving the *P. nodorum* SN15 genome assembly. Joins were either predicted by mesosyntenic patterns or by terminal matches to long insert Sanger sequence reads. Orientations are indicated relative to that of scaffolds of the original assembly.

Center scaffold	Right scaffold	Orientation	Evidence
scaffold_8	scaffold_26	→→	Mesosynteny
scaffold_29	scaffold_48	←←	Mesosynteny
scaffold_37	scaffold_48	→→	Mesosynteny
scaffold_51	scaffold_55	←←	Mesosynteny
scaffold_2	scaffold_107	←→	Long-insert library
scaffold_7	scaffold_105	→→	Long-insert library
scaffold_17	scaffold_36	→→	Long-insert library
scaffold_18	scaffold_77	←←	Long-insert library
scaffold_20	scaffold_49	→→	Long-insert library
scaffold_54	scaffold_64	←←	Long-insert library
scaffold_60	scaffold_72	←←	Long-insert library
scaffold_28	scaffold_61	←→	Long-insert library
scaffold_29	scaffold_85	→→	Long-insert library
scaffold_33	scaffold_17	←→	Long-insert library

doi:10.1371/journal.pone.0147221.t002

reading-frame consistency with the remaining spectral matches and new proteins were annotated or existing annotations extended where spectral search results fell outside the coding regions.

Sanger-sequenced reads from previously generated 4 and 10 Kb plasmid and 40 Kb fosmid libraries [26] were aligned to the corrected assembly and paired-end information was used to reassess scaffold joining and orientation (Table 2). We identified read-supported scaffold pairings and orientation by filtering Sanger reads where each read in a pair mapped to a different scaffold, where each of the pairs mapped at only one position in the genome, and where each of the pairs mapped within 40 Kb of the scaffold ends. We excluded scaffold joins where multiple read pairs suggested conflicting pairs or orientation, leaving only unambiguous joins. This process linked 16 scaffolds. Scaffolds 76, 92, and 106 were identified by BLAST as misassembled high-identity matches (>95%) to the mitochondrial genome sequence and were excluded from the nuclear genome assembly.

The repeat content of the new assembly was reassessed. Sub-telomeric repeats R22 and X48 [29] are modestly expanded in the corrected assembly, but repeat content remains largely unchanged (S1 Table).

## Gene Model Correction Summary

After genome corrections, there were 13,563 predicted nuclear genes (Table 3), of which 866 are new genes at new loci and 1,936 are confirmed genes that had been regarded as doubtful in earlier revisions. New loci have been numbered starting at 30,001.

In total, 12,143 (89%) genes in the current list possess some form of experimental supporting evidence (Fig 1). Microarray probe intensity supported the transcription of 9,961 loci. RNA-seq supported the exon structure of 10,544 gene models, including 299 loci with at least one alternatively spliced transcript, encoding a total of 13,949 proteins. 8,366 existing genes have had their protein sequence modified, 1,936 previously deprecated loci have been reinstated, and 866 new genes were introduced when the previous genome annotation had incorrectly split genes (55 occurrences, S2A Table), joined genes (356 occurrences, S2B Table) or where there was no previous annotation (455 occurrences) (Table 3, S3 Table). Four intronic endonuclease [64, 65] insertion events were annotated where an open reading frame occurred

Table 3. Summary of the characteristics of annotated *P. nodorum* SN15 genes and their protein products before and after manual re-annotation. Manually-annotated genes are longer, have more annotated transcripts, are more likely to accord with proteomic data, and are more likely to have conserved protein domains.

	Before	After
Gene model count	12,199	13,569
Average exon count	2.6	2.5
Average CDS length (bp)	1,271.4	1,368.7
Intergenic distance mean (bp)	600	1010
Intergenic distance std dev (bp)	1,616	2,057
Intron length mean (bp)	89.9	66.6
Intron length std dev (bp)	84.3	52.4
Proteins with Pfam domains	11,464	13,248
Proteins with Gene3D domains	11,287	13,184
Proteins with SignalP predictions	1,122	1,476
Models with peptide support	2,665	4,352
Models with peptide conflict	150	0
Genes with alternative transcripts	0	299

doi:10.1371/journal.pone.0147221.t003
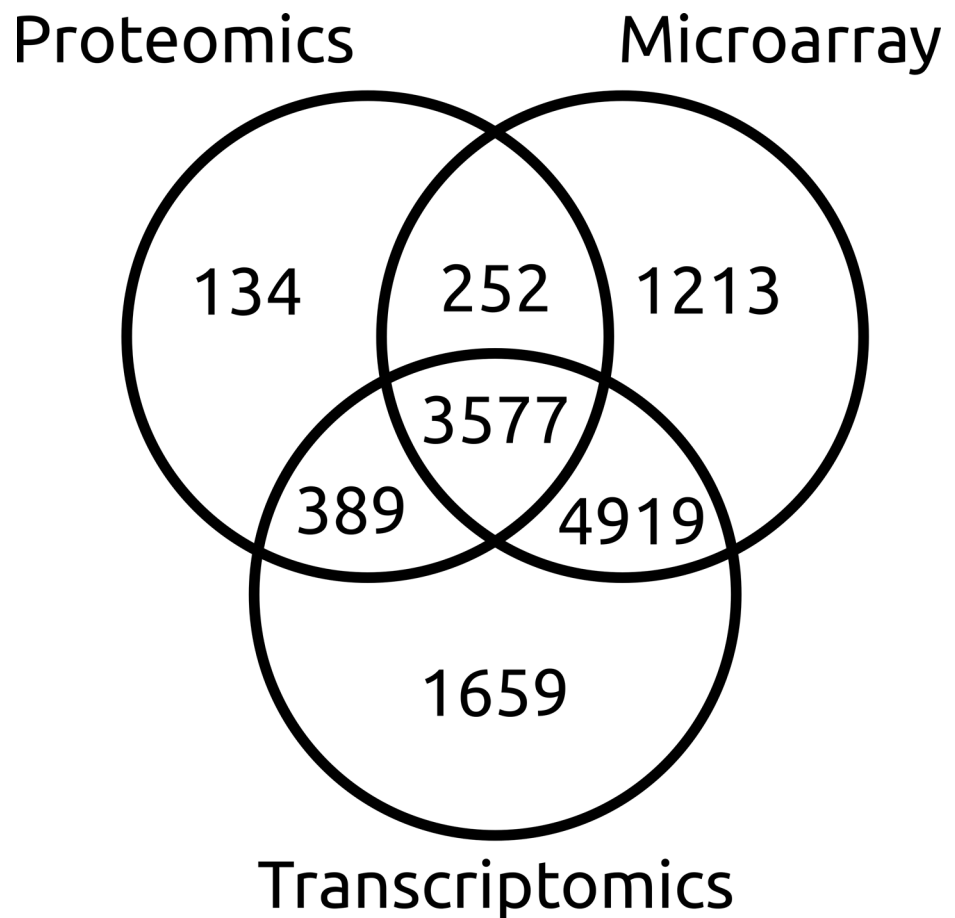
Fig 1. Sources of evidence used to re-annotate *P. nodorum* SN15 genes. This data supported 12,143 annotations with at least one source of experimental support. Additional annotations were also supported by non-experimental sources including the presence of conserved domains or homology to genes of other species.

doi:10.1371/journal.pone.0147221.g001
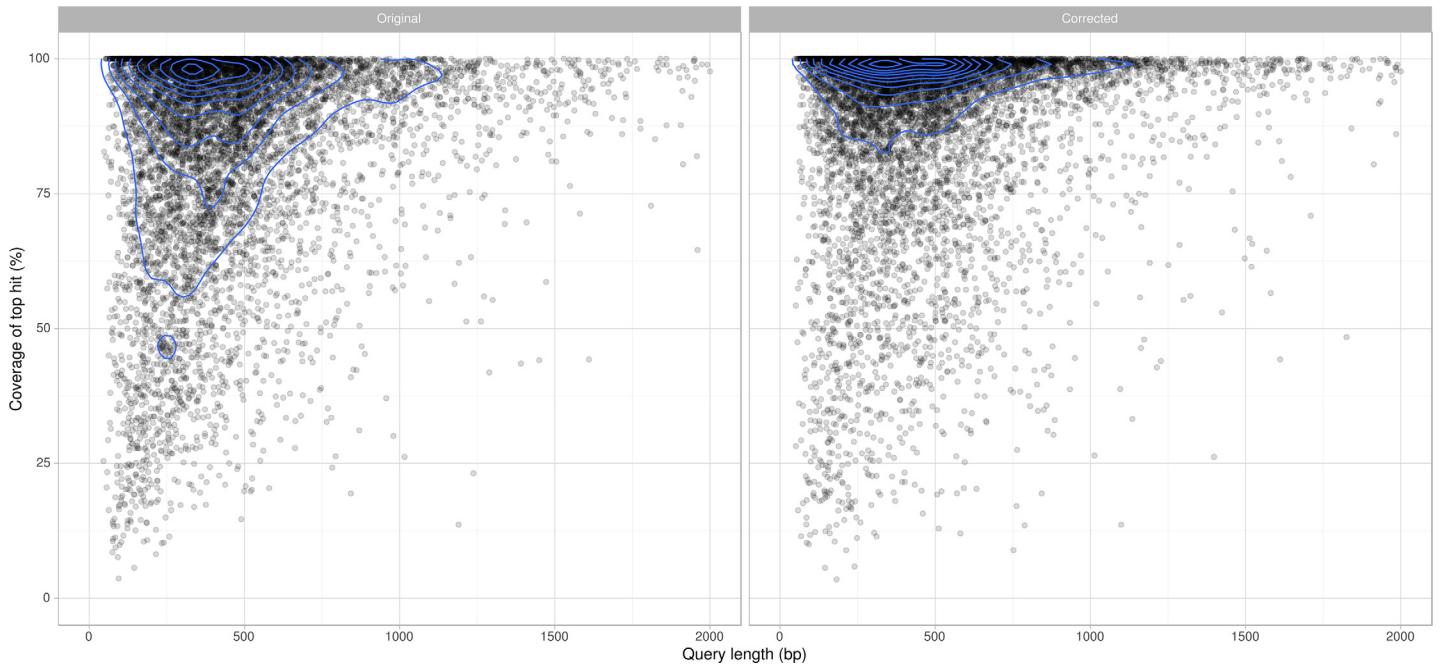
Fig 2. Coverage of the top BLASTP hit for re-annotated *P. nodorum* SN15 predicted proteins. The manually curated set (left) agrees more closely with sequences in the NCBI Protein NR database than the original set of annotations (right). Contour lines (blue) indicate 'kernel density', depicting the relative number of proteins within a localised region of the plot.

within another gene (*SNOG_30297*, *SNOG_30841*, *SNOG_14322*, and *SNOG_16073*). BLAST analysis of the inserted endonuclease protein sequences to the NCBI non-redundant protein database returned only hits to fragments of loci annotated as the host gene.

A core set of 11,849 protein clusters present in all three *P. nodorum* strains were identified by combining orthologous proteins using ProteinOrtho. Inputs were the improved set of SN15 annotations (13,949 proteins) and the proteomes of SN4 and SN79 re-annotated based on the new reference gene models (13,899 proteins and 13,746 proteins respectively).

Functional Annotation Improvements

Comparison of each predicted protein to their top BLAST hit not belonging to the *Parastagonospora* genus reveals the new annotation set to be more concordant with annotations in other species ([Fig 2](#)). In particular, we observed a dramatic shift from shorter annotations to longer annotations that represent a higher proportion of the length of their best-matching homolog. Manual correction has eliminated occurrences of conflict between the predicted protein set and the mapped location of proteomic spectra ([Table 3](#)).

Compared to the gene annotations from Bringans et al. [27], the new set includes 1,784 more proteins with predicted Pfam domains [66], 1,897 more with Gene3D domains [67], and 354 more with SignalP-predicted signal peptides [68] ([Table 3](#)). CAZyme classifications show an increase in the number of proteins belonging to the carbohydrate-binding module (46), carbohydrate esterase (32), glycoside hydrolase (16), and glycosyl transferase (9) families after re-annotation ([Table 4](#)).

Genes and Domains of Interest

Known *P. nodorum* effectors ToxA, Tox1, and Tox3 are not homologous but do share common characteristics. They are small (13 kDa, 10 kDa and 17 kDa respectively), contain signal

Table 4. Summary of carbohydrate-active enzyme (CAZyme) family numbers in *P. nodorum* SN15 before and after manual re-annotation.

CAZyme Family		Original match count	Corrected match count
Auxiliary Activity	AA	122	139
Carbohydrate-Binding Module Family	CBM	64	110
Carbohydrate Esterase Family	CE	142	174
Dockerin	-	1	1
Glycoside Hydrolase Family	GH	264	280
Glycosyl Transferase Family	GT	96	105
Polysaccharide Lyase	PL	10	10

doi:10.1371/journal.pone.0147221.t004

peptides to target the protein to the secretory system and contain cysteine residues which may form disulphide bridges that help maintain protein stability once secreted. Their genes are positioned close to repeats. It has been suggested that effector proximity to repeats may expose them to an elevated level of mutation due to leakage of the RIP process outside truly repetitive sequence [69]. The known *P. nodorum* effectors are absent from the SN79 strain, and are highly expressed early in infection [15]. Among the 866 proteins annotated at new loci are proteins enriched in the properties of known necrotrophic effectors. This includes elevated cysteine content that may facilitate disulphide bridge formation for extracellular structural stability [70]. The newly annotated proteins have products with higher average cysteine content than the unchanged or modified proteins (Fig 3). Of the 54 proteins in the corrected set with more than 9% cysteine content, 16 are from genes at previously unannotated loci, and 51 have no BLAST match in to the NCBI Protein database (Table 4). The corrected set revealed 187 extra proteins with BLAST hits to entries in the PHIbase pathogen-host interaction database [71] that are experimentally shown to influence pathogenicity. Included among the cysteine-rich genes at new loci is a putative degraded copy of *P. nodorum* effector gene *Tox1* (Table 5, S4 Table). Effectors and other components of pathogenicity are likely to be members of the set of 2,169 protein clusters present in at least one wheat pathogen but absent from the avirulent SN79 strain.

All but one of the polyketide synthase (PKS) genes have had their gene structure modified (Table 6, S1 Fig). The modified protein models were used by Chooi, Muria-Gonzalez [72] to identify 24 PKS genes with one type III PKS, one hybrid non-ribosomal peptide synthetase/PKS, one partially reducing PKS, 7 non-reducing PKSs, and 14 highly reducing PKSs. Two extra proteins with putative pathogenicity domains HCE2 [Pfam: PF14856] and Ricin-type beta-trefoil lectin [Pfam: PF00652] are uncovered in the new protein set (Table 7, S4 Table), the latter of which has also been identified as a potentially important pathogenicity factor in another fungal wheat pathogen *Rhizoctonia solani* AG8-1 [73]. Overall, Pfam domains with an increased representation in the new protein set include DNA-binding domains (117), transcription factors (51) and chitin-binding sequence (21).

Discussion

The completeness and accuracy of an organism's reference genome sequence and its gene annotations directly influence the validity of computational and reverse genetics-based downstream functional studies. This is especially relevant in plant pathology, for which considerable research efforts are invested into predicting and functionally characterising putative effector genes from genomic datasets. Identification of effectors and subsequent effector-assisted breeding programs have been an important contribution to crop protection against pathogens [74]. Screening of potential lines with a purified effector negates or diminishes the need for more
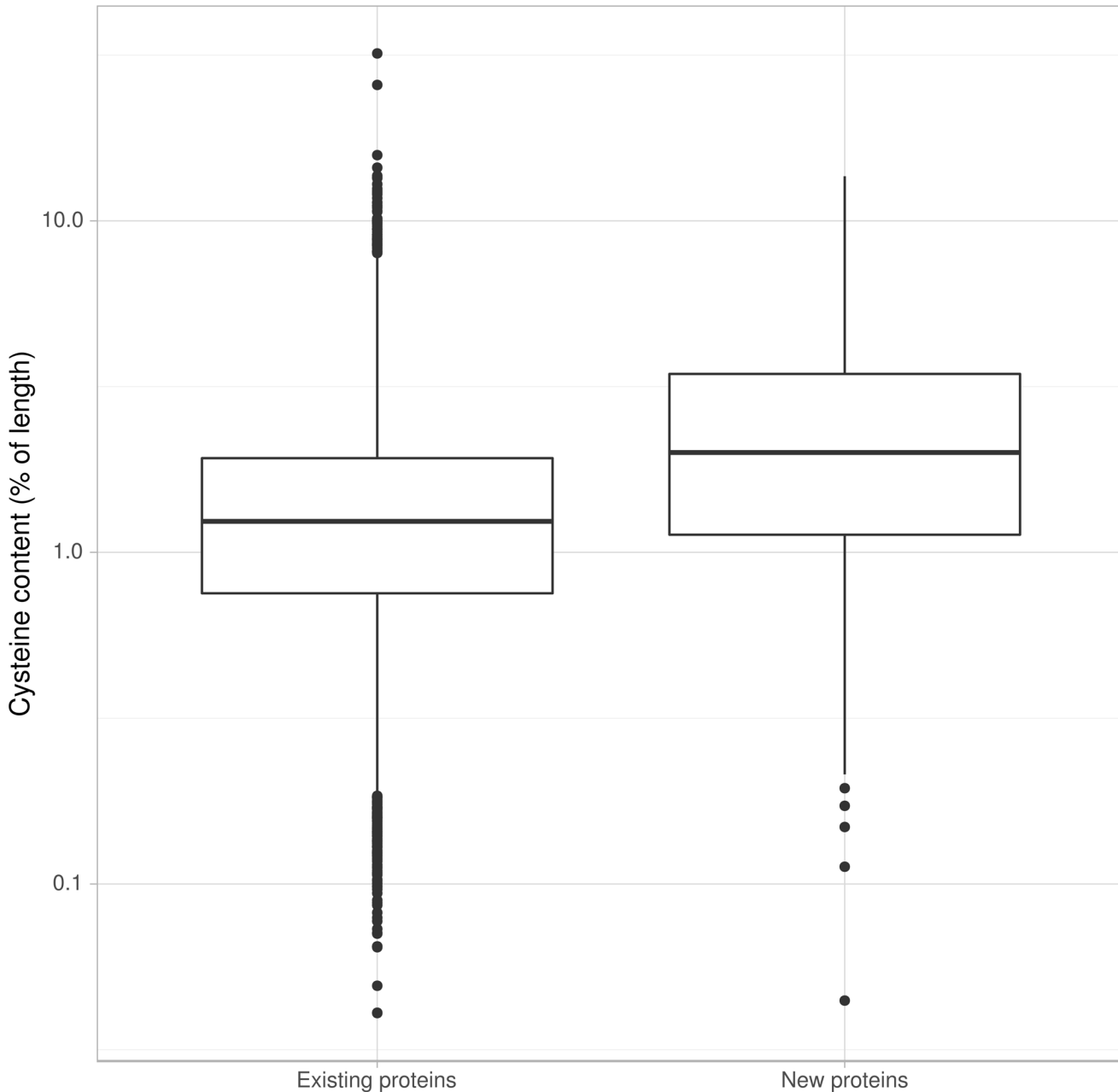
Fig 3. Proportion of cysteines in *P. nodorum* SN15 predicted proteins before and after gene re-annotation. New proteins are more likely to be cysteine-rich. Of the 54 cysteine-rich proteins in the new annotation set (> 9% Cys by length), 16 are the products of newly annotated loci.

costly and time-consuming infection assays and field trials. Analysis based on protein sequence such as effector prediction or functional annotation rely on accurate gene models, and by extension, assembly sequence.

For example, insertion and deletion errors in the underlying assembly sequence can force automated gene calling software to introduce erroneous intron features in order to extend an open-reading frame. This can lead to an inflated exon count and interrupt BLAST and/or protein domain matches, which can impair assignment of biologically relevant functional terms to genes [73].

Table 5. Summary of cysteine-rich protein-products of previously unannotated genes in *P. nodorum* SN15. Novel cysteine-rich annotations have few BLAST hits and include potential effector candidate genes e.g. *SNOG_30451*- a degraded and truncated homolog of *Tox1*.

Gene name	Protein length	Cysteine count	Cysteine percentage	Blast hits
SNOR_30077	66	9	13.6	No
SNOR_30525	74	10	13.5	No
SNOR_30316	94	11	11.7	No
SNOR_30335	70	8	11.4	No
SNOR_30888	53	6	11.3	No
SNOR_30837	56	6	10.7	No
SNOR_30741	355	37	10.4	Carbohydrate-binding
SNOR_30253	58	6	10.3	No
SNOR_30352	79	8	10.1	No
SNOR_30019	60	6	10	No
SNOR_30451	62	6	9.7	Fungal hypothetical genes
SNOR_30925	104	10	9.6	No
SNOR_30828	84	8	9.5	No
SNOR_30466	84	8	9.5	Tox1
SNOR_30530	76	7	9.2	No
SNOR_30989	55	5	9.1	No

doi:10.1371/journal.pone.0147221.t005

Table 6. Polyketide synthase genes of *P. nodorum* SN15.

Gene name	PKS Type
SNOG_09622	Type III PKS
SNOR_00308	Hybrid Nonribosomal peptide synthetase/PKS
SNOR_00477	Partially reducing-PKS
SNOR_02561	Highly reducing-PKS
SNOR_04868	Highly reducing -PKS
SNOR_05791	Highly reducing -PKS
SNOR_06676	Highly reducing -PKS
SNOR_07866	Highly reducing -PKS
SNOR_09623	Highly reducing -PKS
SNOR_11066	Highly reducing -PKS
SNOR_11076	Highly reducing -PKS
SNOR_11272	Highly reducing -PKS
SNOR_12897	Highly reducing -PKS
SNOR_13032	Highly reducing -PKS
SNOR_14927	Highly reducing -PKS
SNOR_15965	Highly reducing -PKS
SNOG_09490	Highly reducing -PKS
SNOR_06682	Non-reducing -PKS
SNOR_07020	Non-reducing -PKS
SNOR_11981	Non-reducing -PKS
SNOR_15829	Non-reducing -PKS
SNOR_08274	Non-reducing -PKS
SNOG_08614	Non-reducing -PKS
SNOG_09932	Non-reducing -PKS

doi:10.1371/journal.pone.0147221.t006

Table 7. Summary of changes to protein-products with functional annotations of high relevance to plant pathogenicity in *P. nodorum* SN15, before and after re-annotation.

Pfam ID	Domain name	Before	After
PF14856	Hce2	1	2
PF00652	Ricin_B_lectin	0	1
PF00188	CAP	4	4
PF10167	NEP	0	0
PF01476	LysM	2	2
PF05630	NPP1	2	2
PF11584	Toxin_ToxA	1	1

doi:10.1371/journal.pone.0147221.t007

A number of corrections have been made to the *P. nodorum* SN15 genome assembly, reducing the number of nuclear scaffolds from 107 to 91. SNP and indel removal facilitated by the addition of the Illumina data allowed a re-evaluation of the long-range paired end Sanger read
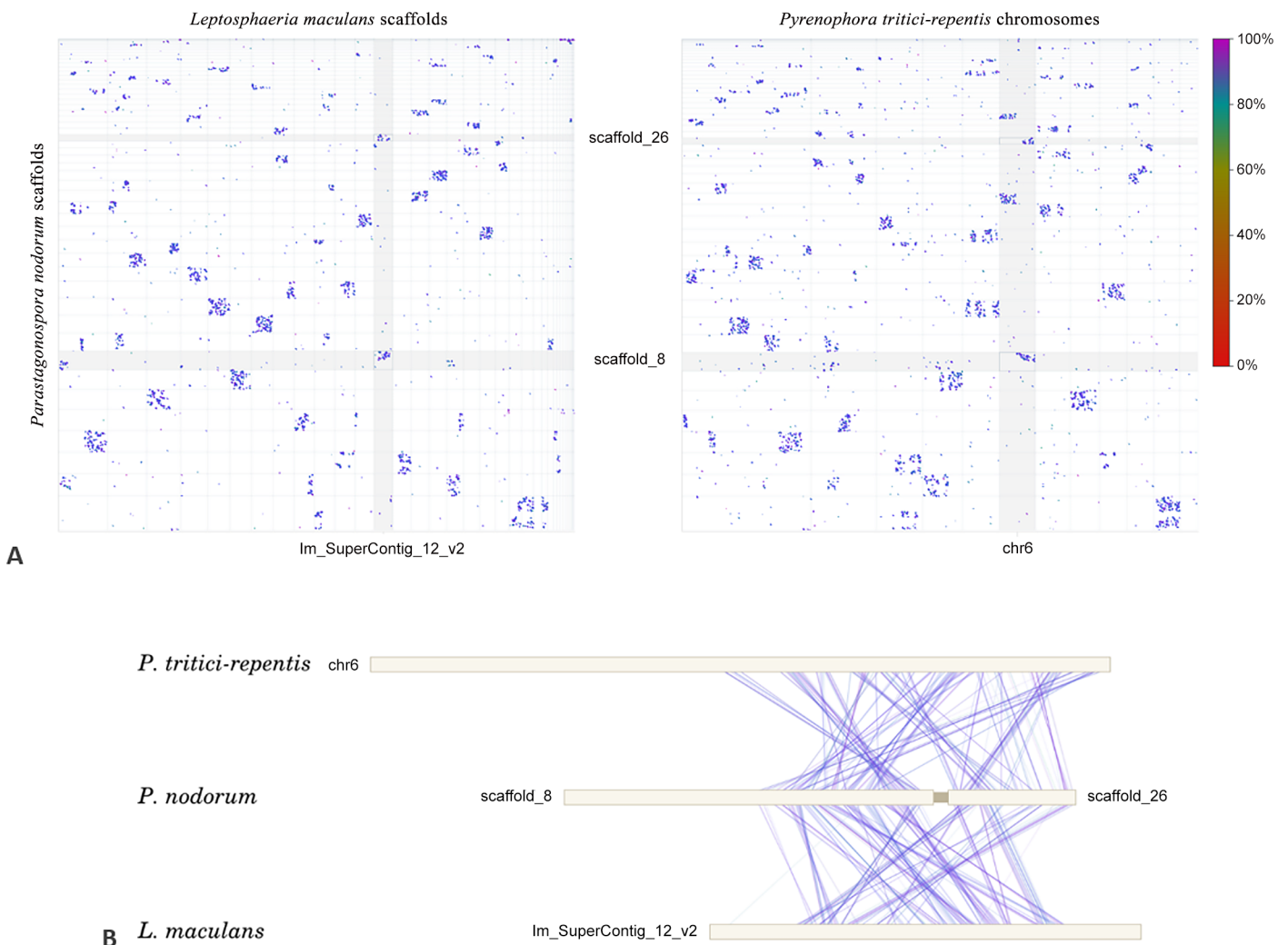
Fig 4. A whole-genome dotplot of nucmer matches between scaffolds of *P. nodorum* and of *P. tritici-repentis*. The 'dots-in-boxes' pattern is indicative of mesosyntenic relationships between chromosomes. *P. nodorum* scaffolds 8 and 26 are 'mesosyntenic' versus *P. tritici-repentis* scaffold 4, as indicated by black boxes.

doi:10.1371/journal.pone.0147221.g004

data which, in turn, permitted the confident joining of 8 pairs of scaffolds. Eight scaffolds were joined that exhibited mesosyntenic relationships ([Table 2](#)). Scaffolds 8 and 26, for example both show mesosyntenic similarity to scaffold 4 on *P. tritici-repentis* ([Fig 4](#)). Joining scaffolds adds to our knowledge of the genomic context of particular regions of the genome, including the 'transfercon' harbouring the *ToxA* gene [8, 31, 32]. Confirmation of the scaffold 55/51 join predicted by mesosyntenic pairings and by homology to the *ToxA* region in *P. tritici-repentis* [31] lends support to the theory of an expanded 72 Kb transfercon and subsequent repeat invasion in *P. nodorum*. Pulsed field gel electrophoresis has been previously used to resolve between 14 and 19 chromosomes from different *P. nodorum* isolates [75]. Hence, a substantial number of gaps still remained unresolved in the current assembly.

In addition to improvements in existing genes, manual annotation has also uncovered genes at new loci. Many of these new genes are small and cysteine-rich ([Table 5](#)) with few BLAST hits to the NCBI protein database–hallmark characteristics of proteins involved in pathogenicity [31] and are effector candidates. Further evidence that these are relevant effectors could be obtained by determining whether they are expressed *in planta*.

The errors in the *P. nodorum* SN15 assembly sequence and its genome annotations are not unusual for a genome project of its age, assembly strategy and sequencing history. Similar fungal genome projects lacking 'multi-omics'-based evidence may therefore harbour undiscovered annotation and sequencing errors, adversely affecting the accuracy of their genome analysis and the accuracy of comparative genomics studies in which they have been used.

We present an integrated analysis of multiple genomic, transcriptomic and proteomic datasets and their application to the improvement of the genome assembly and gene annotations of the fungal pathogen *P. nodorum* SN15. Experimental approaches undertaken in this study can readily be applied to other biological systems to refine gene models and assist in the assembly of uncompleted genomes. We anticipate that others establishing fungal genome projects would similarly benefit from the techniques described in this study.

Supporting Information

S1 Fig. Details of polyketide synthase genes before and after correction.
(DOCX)

S1 Table. Re-annotated repetitive content in updated genome assembly of *P. nodorum* SN15.
(DOCX)

S2 Table. Details of modified gene annotations. A) Genes that are a product of merging two or more annotations. B) Genes that are a product of splitting one annotation into two or more genes.
(DOCX)

S3 Table. Details of new gene annotations.
(DOCX)

S4 Table. Details of cysteine-rich protein properties, matches to PHIbase and changes in functional annotations.
(DOCX)

S1 Text. Supplementary Methods: Illumina read QC and trimming parameters.
(DOCX)

Acknowledgments

Author Contributions

Conceived and designed the experiments: RAS KCT JKH RPO. Performed the experiments: RAS KCT KD TS MH EF SRE AHW YFT JJG. Analyzed the data: RAS JKH. Contributed reagents/materials/analysis tools: RAS ACT JKH. Wrote the paper: RAS JKH KCT KD TS MH SRE AHW YFT ACT JJG RPO.

References

1. Chain P, Grafham D, Fulton R, Fitzgerald M, Hostetler J, Muzny D, et al. Genome project standards in a new era of sequencing. Science. 2009; 326(5950).

2. Murray GM, Brennan JP. Estimating disease losses to the Australian wheat industry. Australasian Plant Pathology. 2009; 38:558–70.

3. Crook A, Friesen T, Liu Z, Ojiambo P, Cowger C. Novel necrotrophic effectors from Stagonospora nodorum and corresponding host sensitivities in winter wheat germplasm in the southeastern United States. Phytopathology. 2012; 102(5):498–505. doi: 10.1094/PHYTO-08-11-0238 PMID: 22494247

4. Stergiopoulos I, Collemare J, Mehrabi R, De Wit PJ. Phytotoxic secondary metabolites and peptides produced by plant pathogenic Dothideomycete fungi. FEMS microbiology reviews. 2013; 37(1):67–93. doi: 10.1111/j.1574-6976.2012.00349.x PMID: 22931103

5. Quaedvlieg W, Verkley G, Shin H-D, Barreto R, Alfenas A, Swart W, et al. Sizing up Septoria. Studies in Mycology. 2013; 75:307–90. doi: 10.3114/sim0017 PMID: 24014902

6. Solomon P, Waters O, Jorgens C, Lowe R, Rechberger J, Trengove R, et al. Mannitol is required for asexual sporulation in the wheat pathogen Stagonospora nodorum (glume blotch). Biochem J. 2006; 399:231–9. PMID: 16859492

7. Tan KC, Oliver RP, Solomon PS, Moffat CS. Proteinaceous necrotrophic effectors in fungal virulence. Functional Plant Biology. 2010; 37:907–12.

8. Friesen TL, Stukenbrock EH, Liu Z, Meinhardt S, Ling H, Faris JD, et al. Emergence of a new disease as a result of interspecific virulence gene transfer. Nature Genetics. 2006; 38(8):953–6. PMID: 16832356

9. Liu Z, Faris J, Meinhardt S, Ali S, Rasmussen J, Friesen T. Genetic and physical mapping of a gene conditioning sensitivity in wheat to a partially purified host-selective toxin produced by Stagonospora nodorum. Phytopathology. 2004; 94(10):1056–60. doi: 10.1094/PHYTO.2004.94.10.1056 PMID: 18943793

10. Liu Z, Faris JD, Oliver RP, Tan KC, Solomon PS, McDonald MC, et al. SnTox3 acts in effector triggered susceptibility to induce disease on wheat carrying the Snn3 gene. PLoS Pathogens. 2009; 5(9): e1000581. doi: 10.1371/journal.ppat.1000581 PMID: 19806176

11. Friesen TL, Faris JD, Solomon PS, Oliver RP. Host-specific toxins: effectors of necrotrophic pathogenicity. Cellular microbiology. 2008; 10(7):1421–8. doi: 10.1111/j.1462-5822.2008.01153.x PMID: 18384660

12. Tan K-C, Waters OD, Rybak K, Antoni E, Furuki E, Oliver RP. Sensitivity to three Parastagonospora nodorum necrotrophic effectors in current Australian wheat cultivars and the presence of further fungal effectors. Crop and Pasture Science. 2014; 65(2):150–8.

13. Solomon PS, Lee RC, Wilson T, Oliver RP. Pathogenicity of Stagonospora nodorum requires malate synthase. Molecular microbiology. 2004; 53(4):1065–73. PMID: 15306011

14. Solomon PS, Jörgens CI, Oliver RP. δ-Aminolaevulinic acid synthesis is required for virulence of the wheat pathogen Stagonospora nodorum. Microbiology. 2006; 152(5):1533–8.

15. Ipcho SV, Hane JK, Antoni EA, Ahren D, Henrissat B, Friesen TL, et al. Transcriptome analysis of Stagonospora nodorum: gene models, effectors, metabolism and pantothenate dispensability. Molecular plant pathology. 2012; 13(6):531–45. doi: 10.1111/j.1364-3703.2011.00770.x PMID: 22145589

16. Lowe RG, Lord M, Rybak K, Trengove RD, Oliver RP, Solomon PS. Trehalose biosynthesis is involved in sporulation of Stagonospora nodorum. Fungal Genetics and Biology. 2009; 46(5):381–9. doi: 10.1016/j.fgb.2009.02.002 PMID: 19233304

17. Solomon PS, Tan K-C, Oliver RP. Mannitol 1-phosphate metabolism is required for sporulation in planta of the wheat pathogen Stagonospora nodorum. Molecular Plant-Microbe Interactions. 2005; 18 (2):110–5. PMID: 15720079

18. IpCho SV, Tan K-C, Koh G, Gummer J, Oliver RP, Trengove RD, et al. The transcription factor StuA regulates central carbon metabolism, mycotoxin production, and effector gene expression in the wheat pathogen Stagonospora nodorum. Eukaryotic cell. 2010; 9(7):1100–8. doi: 10.1128/EC.00064-10 PMID: 20495056

19. Solomon PS, Waters OD, Simmonds J, Cooper RM, Oliver RP. The Mak2 MAP kinase signal transduction pathway is required for pathogenicity in Stagonospora nodorum. Current genetics. 2005; 48(1):60–8. PMID: 16028107

20. Solomon PS, Rybak K, Trengove RD, Oliver RP. Investigating the role of calcium/calmodulin-dependent protein kinases in Stagonospora nodorum. Molecular microbiology. 2006; 62(2):367–81. PMID: 17020577

21. Tan K-C, Heazlewood JL, Millar AH, Thomson G, Oliver RP, Solomon PS. A signaling-regulated, short-chain dehydrogenase of Stagonospora nodorum regulates asexual development. Eukaryotic cell. 2008; 7(11):1916–29. doi: 10.1128/EC.00237-08 PMID: 18776038

22. Casey T, Solomon PS, Bringans S, Tan KC, Oliver RP, Lipscombe R. Quantitative proteomic analysis of G-protein signalling in Stagonospora nodorum using isobaric tags for relative and absolute quantification. Proteomics. 2010; 10(1):38–47. doi: 10.1002/pmic.200900474 PMID: 19882661

23. Tan KC, Trengove RD, Maker GL, Oliver RP, Solomon PS. Metabolite profiling identifies the mycotoxin alternariol in the pathogen Stagonospora nodorum. Metabolomics. 2009:1–6.

24. Solomon PS, Tan K-C, Sanchez P, Cooper RM, Oliver RP. The disruption of a Gα subunit sheds new light on the pathogenicity of Stagonospora nodorum on wheat. Molecular Plant-Microbe Interactions. 2004; 17(5):456–66. PMID: 15141949

25. Gummer JP, Trengove RD, Oliver RP, Solomon PS. A comparative analysis of the heterotrimeric G-protein Gα, Gβ and Gγ subunits in the wheat pathogen Stagonospora nodorum. BMC microbiology. 2012; 12(1):131.

26. Hane JK, Lowe RG, Solomon PS, Tan KC, Schoch CL, Spatafora JW, et al. Dothideomycete plant interactions illuminated by genome sequencing and EST analysis of the wheat pathogen Stagonospora nodorum. The Plant Cell. 2007; 19(11):3347–68. PMID: 18024570.

27. Bringans S, Hane JK, Casey T, Tan KC, Lipscombe R, Solomon PS, et al. Deep proteogenomics; high throughput gene validation by multidimensional liquid chromatography and mass spectrometry of proteins from the fungal wheat pathogen Stagonospora nodorum. BMC Bioinformatics. 2009; 10:301. doi: 10.1186/1471-2105-10-301 PMID: 19772613

28. Ipcho SVS, Hane JK, Antoni EA, Ahren D, Henrissat B, Friesen TL, et al. Transcriptome analysis of Stagonospora nodorum: Gene models, effectors, metabolism and pantothenate dispensability. Molecular Plant Pathology. 2012; 13(6):531–45. doi: 10.1111/j.1364-3703.2011.00770.x PMID: 22145589

29. Hane JK, Lowe RG, Solomon PS, Tan K-C, Schoch CL, Spatafora JW, et al. Dothideomycete–plant interactions illuminated by genome sequencing and EST analysis of the wheat pathogen Stagonospora nodorum. The Plant Cell Online. 2007; 19(11):3347–68.

30. Hane JK, Oliver RP. In silico reversal of repeat-induced point mutation (RIP) identifies the origins of repeat families and uncovers obscured duplicated genes. BMC Genomics. 2010; 11:655. doi: 10.1186/1471-2164-11-655 PMID: 21106049

31. Syme RA, Hane JK, Friesen TL, Oliver RP. Resequencing and comparative genomics of Stagonospora nodorum: Sectional gene absence and effector discovery. G3: Genes| Genomes| Genetics. 2013; 3 (6):959–69. doi: 10.1534/g3.112.004994 PMID: 23589517

32. Manning VA, Pandelova I, Dhillon B, Wilhelm LJ, Goodwin SB, Berlin AM, et al. Comparative genomics of a plant-pathogenic fungus, Pyrenophora tritici-repentis, reveals transduplication and the impact of repeat elements on pathogenicity and population divergence. G3: Genes| Genomes| Genetics. 2013; 3 (1):41–63.

33. Shendure J, Ji H. Next-generation DNA sequencing. Nature biotechnology. 2008; 26(10):1135–45. doi: 10.1038/nbt1486 PMID: 18846087

34. Zhang J, Chiodini R, Badr A, Zhang G. The impact of next-generation sequencing on genomics. Journal of Genetics and Genomics. 2011; 38(3):95–109. doi: 10.1016/j.jgg.2011.02.003 PMID: 21477781

35. Chevreux B, Wetter T, Suhai S, editors. Genome sequence assembly using trace signals and additional sequence information. German Conference on Bioinformatics; 1999.

36. Grandaubert J, Bhattacharyya A, Stukenbrock EH. RNA-seq Based Gene Annotation and Comparative Genomics of Four Fungal Grass Pathogens in the Genus Zymoseptoria Identify Novel Orphan Genes and Species-Specific Invasions of Transposable Elements. G3: Genes| Genomes| Genetics. 2015:g3. 115.017731.

37. Hane JK, Rouxel T, Howlett BJ, Kema GH, Goodwin SB, Oliver RP. A novel mode of chromosomal evolution peculiar to filamentous Ascomycete fungi. Genome Biol. 2011; 12(5):R45. doi: 10.1186/gb-2011-12-5-r45 PMID: 21605470

38. Ohm RA, Feau N, Henrissat B, Schoch CL, Horwitz BA, Barry KW, et al. Diverse lifestyles and strategies of plant pathogenesis encoded in the genomes of eighteen Dothideomycetes fungi. PLoS Pathogens. 2012; 8(12):e1003037. doi: 10.1371/journal.ppat.1003037 PMID: 23236275

39. Liu ZH, Faris JD, Meinhardt SW, Ali S, Rasmussen JB, Friesen TL. Genetic and physical mapping of a gene conditioning sensitivity in wheat to a partially purified host-selective toxin produced by Stagonospora nodorum. Phytopathology. 2004; 94(10):1056–60. PMID: CCC:000224069000004. doi: 10.1094/PHYTO.2004.94.10.1056

40. Clarke JD. Cetyltrimethyl ammonium bromide (CTAB) DNA miniprep for plant DNA isolation. Cold Spring Harb Protoc. 2009;2009:pdb prot5177. Epub 2010/02/12. doi: 10.1101/pdb.prot5177 PMID: 20147112.

41. Tan KC, Heazlewood JL, Millar AH, Thomson G, Oliver RP, Solomon PS. A signaling-regulated, short-chain dehydrogenase of Stagonospora nodorum regulates asexual development. Eukaryotic Cell. 2008; 7(11):1916–29. doi: 10.1128/EC.00237-08 PMID: 18776038

42. Andrews S. FastQC: A quality control tool for high throughput sequence data. Reference Source. 2010.

43. Martin M. Cutadapt removes adapter sequences from high-throughput sequencing reads. EMBnet journal. 2011; 17(1):pp. 10–2.

44. Vincent D, Tan KC, Cassidy L, Solomon PS, Oliver RP. Proteomic techniques for plant-fungal interactions. Methods Mol Biol. 2012; 835:75–96. Epub 2011/12/21. doi: 10.1007/978-1-61779-501-5_5 PMID: 22183648.

45. Hastie ML, Headlam MJ, Patel NB, Bukreyev AA, Buchholz UJ, Dave KA, et al. The human respiratory syncytial virus nonstructural protein 1 regulates type I and type II interferon pathways. Molecular & Cellular Proteomics. 2012; 11(5):108–27.

46. Diament BJ, Noble WS. Faster SEQUEST searching for peptide identification from tandem mass spectra. Journal of proteome research. 2011; 10(9):3871–9. doi: 10.1021/pr101196n PMID: 21761931

47. Park CY, Klammer AA, Käll L, MacCoss MJ, Noble WS. Rapid and accurate peptide identification from tandem mass spectra. Journal of proteome research. 2008; 7(7):3022–7. doi: 10.1021/pr800127y PMID: 18505281

48. Käll L, Canterbury JD, Weston J, Noble WS, MacCoss MJ. Semi-supervised learning for peptide identification from shotgun proteomics datasets. Nature methods. 2007; 4(11):923–5. PMID: 17952086

49. Casey T, Solomon PS, Bringans S, Tan KC, Oliver RP, Lipscombe R. Quantitative proteomic analysis of G-protein signalling in Stagonospora nodorum using isobaric tags for relative and absolute quantification. Proteomics. 2010; 10:38–47. doi: 10.1002/pmic.200900474 PMID: 19882661

50. Kurtz S, Phillippy A, Delcher AL, Smoot M, Shumway M, Antonescu C, et al. Versatile and open software for comparing large genomes. Genome biology. 2004; 5(2):R12. PMID: 14759262

51. Smit A, Hubley R, Green P. 1996–2010. RepeatMasker Open-3.0. http://www.repeatmaskerorg.

52. Kim D, Pertea G, Trapnell C, Pimentel H, Kelley R, Salzberg SL. TopHat2: accurate alignment of transcriptomes in the presence of insertions, deletions and gene fusions. Genome Biology. 2013; 14(4): R36. doi: 10.1186/gb-2013-14-4-r36 PMID: 23618408

53. Lee E, Helt GA, Reese JT, Munoz-Torres MC, Childers CP, Buels RM, et al. Web Apollo: a web-based genomic annotation editing platform. Genome Biology. 2013; 14:R93. doi: 10.1186/gb-2013-14-8-r93 PMID: 24000942

54. Skinner ME, Uzilov AV, Stein LD, Mungall CJ, Holmes IH. JBrowse: a next-generation genome browser. Genome research. 2009; 19(9):1630–8. doi: 10.1101/gr.094607.109 PMID: 19570905

55. Jones P, Binns D, Chang H-Y, Fraser M, Li W, McAnulla C, et al. InterProScan 5: genome-scale protein function classification. Bioinformatics. 2014; 30(9):1236–40. doi: 10.1093/bioinformatics/btu031 PMID: 24451626

56. Yin Y, Mao X, Yang J, Chen X, Mao F, Xu Y. dbCAN: a web resource for automated carbohydrate-active enzyme annotation. Nucleic acids research. 2012; 40(W1):W445–W51.

57. Haibao Tang BP, Aurelien Naldi, Patrick Flick, Jeff Yunes, Kenta Sato, Chris Mungall Goatools 2015. Available: https://github.com/tanghaibao/goatools.

58. Holt C, Yandell M. MAKER2: an annotation pipeline and genome-database management tool for second-generation genome projects. BMC bioinformatics. 2011; 12(1):491.

59. Testa AC, Hane JK, Ellwood SR, Oliver RP. CodingQuarry: highly accurate hidden Markov model gene prediction in fungal genomes using RNA-seq transcripts. BMC genomics. 2015; 16(1):170.

60. Lechner M, Findeiß S, Steiner L, Marz M, Stadler PF, Prohaska SJ. Proteinortho: Detection of (Co-) orthologs in large-scale analysis. BMC bioinformatics. 2011; 12(1):124.

61. Tange O. Gnu parallel-the command-line power tool. The USENIX Magazine. 2011; 36(1):42–7.

62. Goto N, Prins P, Nakao M, Bonnal R, Aerts J, Katayama T. BioRuby: Bioinformatics software for the Ruby programming language. Bioinformatics. 2010.

63. Bonnal RJ, Aerts J, Githinji G, Goto N, MacLean D, Miller CA, et al. Biogem: an effective tool based approach for scaling up open source software development in bioinformatics. Bioinformatics. 2012.

64. Belfort M, Roberts RJ. Homing endonucleases: keeping the house in order. Nucleic acids research. 1997; 25(17):3379–88. PMID: 9254693

65. Jin Y, Binkowski G, Simon LD, Norris D. Ho endonuclease cleaves MAT DNA in vitro by an inefficient stoichiometric reaction mechanism. Journal of Biological Chemistry. 1997; 272(11):7352–9. PMID: 9054434

66. Finn RD, Bateman A, Clements J, Coggill P, Eberhardt RY, Eddy SR, et al. Pfam: the protein families database. Nucleic acids research. 2013:gkt1223.

67. Lees JG, Lee D, Studer RA, Dawson NL, Sillitoe I, Das S, et al. Gene3D: Multi-domain annotations for protein sequence and comparative genome analysis. Nucleic acids research. 2014; 42(D1):D240–D5.

68. Bendtsen JD, Nielsen H, von Heijne G, Brunak S. Improved prediction of signal peptides: SignalP 3.0. J Mol Biol. 2004; 340(4):783–95. PMID: 15223320

69. Rouxel T, Grandaubert J, Hane JK, Hoede C, van de Wouw AP, Couloux A, et al. Effector diversification within compartments of the Leptosphaeria maculans genome affected by Repeat-Induced Point mutations. Nature Communications. 2011; 2:202. doi: 10.1038/ncomms1189 PMID: 21326234

70. Stergiopoulos I, de Wit PJ. Fungal effector proteins. Annual review of phytopathology. 2009; 47:233–63. doi: 10.1146/annurev.phyto.112408.132637 PMID: 19400631

71. Urban M, Pant R, Raghunath A, Irvine AG, Pedro H, Hammond-Kosack KE. The Pathogen-Host Interactions database (PHI-base): additions and future developments. Nucleic acids research. 2014: gku1165.

72. Chooi Y-H, Muria-Gonzalez MJ, Solomon PS. A genome-wide survey of the secondary metabolite biosynthesis genes in the wheat pathogen Parastagonospora nodorum. Mycology. 2014; 5(3):192–206. PMID: 25379341

73. Hane JK, Anderson JP, Williams AH, Sperschneider J, Singh KB. Genome Sequencing and Comparative Genomics of the Broad Host-Range Pathogen Rhizoctonia solani AG8. PLoS Genet. 2014; 10(5): e1004281. doi: 10.1371/journal.pgen.1004281 PMID: 24810276

74. Vleeshouwers VG, Oliver RP. Effectors as tools in disease resistance breeding against biotrophic, hemibiotrophic, and necrotrophic plant pathogens. Molecular Plant-Microbe Interactions. 2014; 27 (3):196–206. doi: 10.1094/MPMI-10-13-0313-IA PMID: 24405032

75. Cooley RN, Caten CE. Variation in electrophoretic karyotype between strains of Septoria nodorum. Mol Gen Genet. 1991; 228(1–2):17–23. PMID: 1886607